J Mater Sci (2007) 42:6665–6671
DOI 10.1007/s10853-007-1530-0

Crystallization behaviour and mechanical properties of rapidly solidified $Al_{87.5}Ni_7Mm_5Fe_{0.5}$ amorphous alloy

K. L. Sahoo · P. Poddar · Goutam Das · B. Ravi Kumar

Received: 13 June 2006 / Accepted: 16 January 2007 / Published online: 1 May 2007

Abstract The crystallization behaviour and the mechanical properties of rapidly solidified $Al_{87.5}Ni_7Mm_5Fe_{0.5}$ alloy ribbons have been examined in both as-melt-spun and heat-treated condition using differential scanning calorimetry, X-ray diffractometry (XRD), transmission electron microscopy (TEM), tensile testing and Vicker's microhardness machine. XRD and TEM studies revealed that the as-melt-spun ribbons are fully amorphous. The amorphous ribbon undergoes three-stage crystallization process upon heating. Primary crystallization resulted in the formation of fine nanocrystalline fcc-Al particles embedded in the amorphous matrix. The second and third crystallization stages correspond to the precipitation of $Al_{11}(La,Ce)_3$ and Al_3Ni phases, respectively. Microhardness and tensile strength of the ribbons were examined with the variation of temperature and subsequently correlated with the evolved structure. Initially, the microhardness of the ribbon increases with temperature followed by a sharp drop in hardness owing to the decomposition of amorphous matrix that leads to formation of intermetallic compounds

Introduction

Al-rich (>80 at.%) nanophase composites such as rapidly solidified Al–TM–RE (TM = transition metal, RE = rare earth) alloys have received considerable research interest because of their scientific and technological importance [1–4]. These alloys can be quenched from the melt to a completely amorphous structure [3, 5] or to a mixed structure having uniform distribution of Al nanocrystals in an amorphous matrix [2, 4, 6, 7]. It is well established that the amorphous structure provides higher strength compared to conventional crystalline materials [6]. It has been reported that Al–Ni–Ln (Ln = Y, La or Ce) amorphous alloys exhibit tensile strength above 1000 MPa with good bending ductility, even in Al-rich compositions of 84–86 at.% [3]. On partial crystallization, the nanoscale fcc-Al particles are uniformly dispersed in the amorphous matrix and a higher tensile strength coupled with good ductility is obtained when the volume fraction of the nanoscale Al particles is around 20–30% [3]. It has been reported [3, 8] that the tensile strength is further improved on addition of extra TM *e.g.*, Fe in Al–Ni–RE systems. The ultrafine dislocation-free Al particles are responsible for such a high strength [9, 10]. During the crystallization process the amorphous matrix become enriched in solute elements resulting in an increase of strength [11, 12]. The resulting strength can be described by a simple rule of mixtures involving the strengthened amorphous matrix and the Al nanocrystals of ideal strength [12]. The crystalline particles, smaller than a critical size, become defect-free and its deformation resistance is higher than the amorphous matrix [3]. The mechanical properties and structural evolution of Al–Ni–Ce [8], Al–Ni–Y [4], and Al–Ni–La [3, 7] amorphous alloys have been extensively investigated. Replacement of pure rare earth elements by cost effective rare earth elements such as misch metal (Mm) is potentially attractive and reduces the cost of materials. Some studies [13–17] have been undertaken to investigate the kinetics of the primary crystallization, and mechanical behaviour of amorphous and partially devitrified Al–Ni–Mm alloys.

K. L. Sahoo (✉) · P. Poddar · G. Das · B. R. Kumar
National Metallurgical Laboratory, Jamshedpur 831007, India
e-mail: klsah@nmlindia.org

They reported that the fcc-Al precipitates during the first stage of crystallization. The intermetallic compounds Al_3Ni and $Al_{11}(La,Ce)_3$ precipitate during second and third stages of crystallization, respectively.

In this paper, we report the reverse sequence of precipitation during the second and third stages of crystallization in a rapidly solidified $Al_{87.5}Ni_7Mm_5Fe_{0.5}$ amorphous alloy ribbons. The changes in the microstructure and mechanical properties like strength and bend ductility with temperatures have been reported. Also, the paper reports changes in microhardness as a function of temperature.

Experimental procedure

Ingot of $Al_{87.5}Ni_7Mm_5Fe_{0.5}$ (at.%) was prepared by induction melting in a purified argon atmosphere, taking care that the melt was well inductively stirred to ensure good chemical homogeneity. In order to obtain rapidly solidified ribbons, the ingot was re-melted in an alumina-coated quartz crucible and then ejected through an orifice, at a temperature of 1100 °C, onto a rotating Cu wheel (diameter 300 mm and thickness 38 mm). The ribbons were produced at a wheel speed of 10 m/s, which was the lowest speed in order to get the fully amorphous structure in present experimental condition. All the as-melt-spun ribbons were 12–15 mm wide and 50 ± 5 μm thick. The crystallization temperatures of the samples were measured by differential scanning calorimetry (DSC) using a Perkin-Elmer DSC-7 in flowing argon atmosphere. The amorphous/crystalline natures of the as-melt-spun and heat-treated ribbons were determined by X-ray diffractometry (XRD) and transmission electron microscopy (TEM). The XRD experiments were conducted on a Siemens X-ray diffractometer with Cu Kα radiation (35 kV, 25 mA and scan speed 2 degrees min^{-1}). The specimens for TEM observations were thinned electrolytically in a solution of 25% nitric acid and 75% methanol at –30 °C and 12 V. The hardness of the as-melt-spun and annealed ribbons at various temperature-time combinations was measured by a Vicker's microhardness under a load of 0.196 N (20 gf). The tensile strength was measured using the ribbon specimens with gauge length 25 mm by a Hounsfield tensile testing machine at a strain rate of 4×10^{-4} s^{-1}. In order to measure ductility, bend testing was carried out between the jaws of a digital micrometer, which were slowly closed until the changes in geometry due to onset of plasticity, and later failure occurred. The length of ribbon taken was 30 mm. Bend ductility and the tensile strength data of the ribbons presented are the average of ten measurements excluding those tests where apparently defective samples have detected.

Results and discussion

All the ribbons, produced at 10 m/s, show good bending ductility. They do not break either after bending by 180° or during subsequent re-straightening. Literatures [13, 14, 16] reported the preparation of fully amorphous ribbon at higher speed ranging from 30 to 40 m/s. Figure 1 shows the XRD patterns of the as-melt-spun and annealed (160 °C for 10 min) $Al_{87.5}Ni_7Mm_5Fe_{0.5}$ ribbons. The as-melt-spun sample (Fig. 1a) shows a broad halo centred on $2\theta \approx 37.5^{o}$, which is characteristic of an amorphous phase. Figure 2a shows the bright-field image and selected area diffraction (SAD) pattern of as-melt-spun $Al_{87.5}Ni_7Mm_5Fe_{0.5}$ alloy ribbon. The structure consists of an amorphous single phase as clearly revealed from the SAD pattern. Though the bright-field image contains very faint bright patches, this is due to difference in thickness of the thin foil. XRD pattern (Fig. 1a) also supports this result. Fig. 2b shows the high resolution TEM (HRTEM) image of the annealed sample. It shows changes in microstructure from an amorphous single phase to a mixed structure consisting of nanocrystalline particles dispersed in the amorphous matrix. From the HRTEM study some indication about the size distribution of the nanocrystals could be obtained and they approximately in the range of 3–10 nm as observed from different areas of the sample. The SAD pattern (inset in Fig. 2b) of such nanocrystals revealed fcc type lattice. Energy dispersive X-ray analysis indicated that these crystals contain more Al compared to the amorphous matrix region. The XRD pattern of the annealed samples (Fig. 1b) also confirms mixed structure comprising amorphous and Al-phase. The HRTEM image

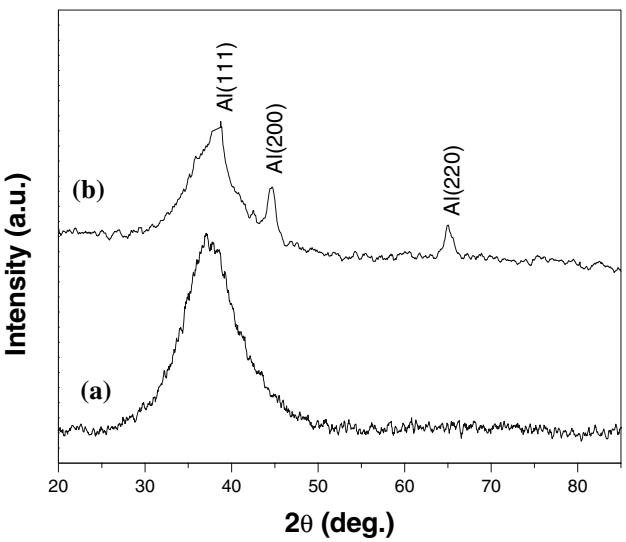

Fig. 1 XRD patterns of $Al_{87.5}Ni_7Mm_5Fe_{0.5}$ ribbons (**a**) as-melt-spun, and (**b**) annealed at 160 °C for 10 min

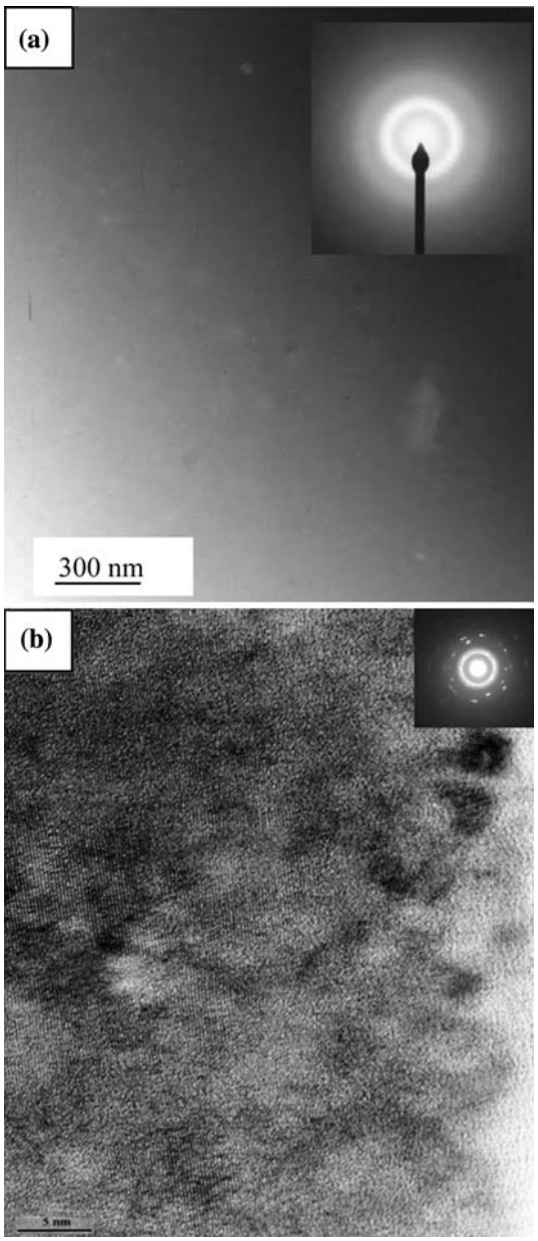

Fig. 2 Bright-field electron diffraction micrographs and selected area diffraction patterns of rapidly solidified $Al_{87.5}Ni_7Mm_5Fe_{0.5}$ alloy (**a**) as-melt-spun, and (**b**) annealed at 160 °C for 10 min

gives partial idea about the crystal orientation, internal structure of Al particles and the interface structure between Al particles and the amorphous matrix. Fig. 2b shows that the Al particles with fringe contrast corresponding to the isolated regions have a nearly spherical or elliptical morphology. No appreciable misfit was seen in the fringe contrast. The nanoscale Al particles appear to have random orientation and distribution with inter particle distance of 2–10 nm. The interface between amorphous matrix and Al particle does not recline on any faceted plane and appears to have a complicated morphology (Fig. 2b).

The continuous heating DSC curve of the as-melt-spun $Al_{87.5}Ni_7Mm_5Fe_{0.5}$ ribbon, at a heating rate of 20 K/min (Fig. 3), shows three exothermal stages, which are attributed to crystallizations. The first stage is somewhat broad with the onset, peak and finish temperature of 155, 185 and 225 °C, respectively. The second and third stages are sharp with peak temperatures of 349 and 363 °C, respectively. Though the as-melt-spun ribbons appeared to be amorphous in XRD study, DSC does not show the presence of a glass transition temperature (T_g). The absence of T_g may be explained that during quenching, while preparing the ribbons, some significant number of cluster distributions may be formed. Literature [7] reports the presence of small clusters by small angle neutron scattering investigation in Al–Ni–La alloys. On heating, the clusters those are above the critical nucleation size grow even at lower temperatures. As a result, T_g is hidden underneath the first crystallization peak. The T_g could not be resolved even with increased heating rate up to 100 K/min. Many of the other metallic glasses also do not show any well-defined T_g in DSC studies [7, 18, 19]. The first crystallization stage of the continuous heating DSC curve showed that the leading edge of the curve is steeper than the trailing edge. The observed shape of the first scanning peak in the present study indicates that the transformation is dominated by grain growth process as reported by Chen and Spaepen [20] for sputtered Al–Mn films.

In order to identify the phases formed at each crystalline stage, different samples were heated, at a rate of 20 K/min,

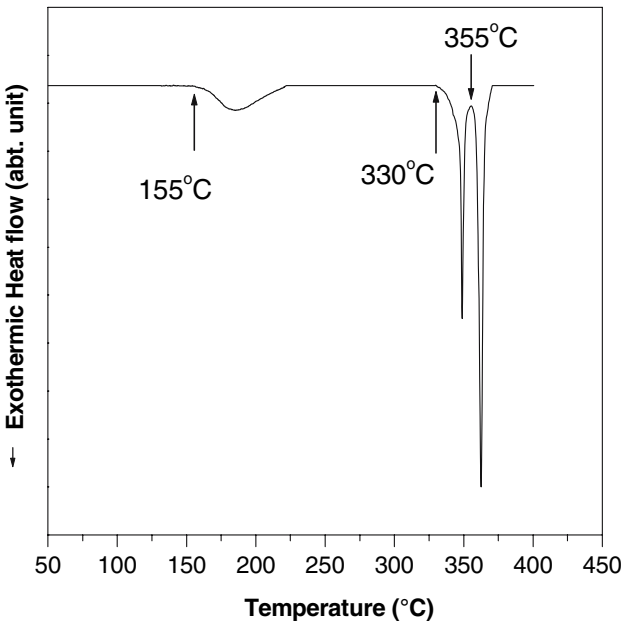

Fig. 3 Continuous heating DSC curve of amorphous $Al_{87.5}Ni_7Mm_5Fe_{0.5}$, at a heating rate of 20 K/min, showing different onset transition temperatures

up to the end of their exothermic reactions (up to ≈325 °C for the first stage, 355 °C for the second stage and 370 °C for the third stage). After heating, the same samples were investigated by XRD. The XRD patterns corresponding to the heat-treated specimen are shown in Fig. 4. The first stage corresponds to the crystallization of fcc-Al from the amorphous matrix. In order to investigate the span of the first crystallization stage, the samples were heated at different temperatures in steps ranging from onset of first crystallization stage (155 °C) to the onset of second crystallization stage (330 °C). The representative XRD patterns are shown in (Figs. 1b and 4). In all the cases (up to 325 °C) only fcc-Al could be detected. The second stage of crystallization corresponds to the precipitation of $Al_{11}(La,Ce)_3$ along with fcc-Al from the amorphous matrix at onset temperature of around 330 °C. The third stage of crystallization corresponds to the precipitation of Al_3Ni from the matrix at onset temperature of around 355 °C (Fig. 4). The observations regarding second and third stages of crystallization products are contradictory to the report published in the literature [13, 14, 17]. They reported second stage corresponds to primarily the crystallization of Al_3Ni and the third stage corresponds to crystallization of $Al_{11}(La,Ce)_3$. However, in order to verify our observations, a series of DSC experiments (for accurate control of temperatures) and XRD studies have been carried out at temperatures starting from the onset temperature of the second crystallization stage i.e. at 330 °C to the finish of third crystallization stage i.e. at 370 °C at an increment of 5 degrees. The representative XRD patterns at few selected temperatures are shown in Fig. 4. The figure

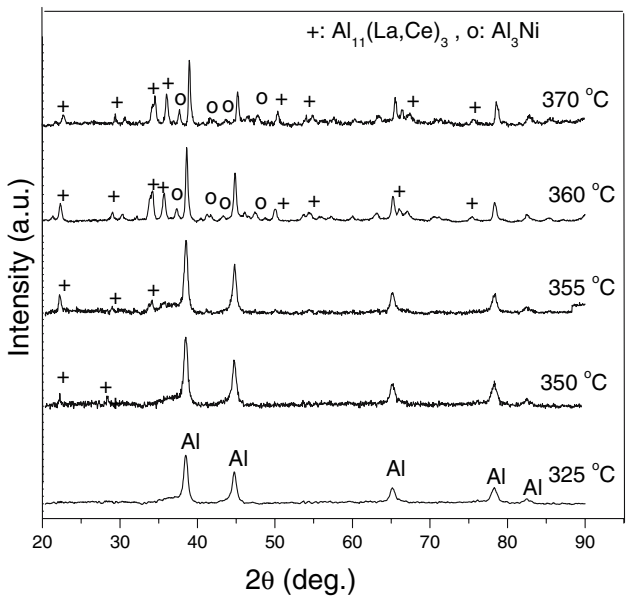

Fig. 4 XRD patterns of the ribbons heated up to different temperatures at a rate of 20 K/min

confirms the occurrence of $Al_{11}(La,Ce)_3$ phase prior to the occurrence of Al_3Ni phase. The transformation temperatures of the crystallization stages in the present investigation are higher than the earlier reported value [17]; possibly due to difference in the chemical compositions of the alloys and the processing conditions. Hawksworth et al. [21] reported that the formation of Al_3Ni or $Al_{11}La_3$ as a first precipitated primary phase from the liquid melt depends on La and Ni content in Al–Ni–La alloy. They reported that Al_3Ni dendrites had higher growth temperature than $Al_{11}La_3$ phase in $Al_{91.8}Ni_{4.3}La_{3.9}$ alloy. In a hypoeutectic (eutectic composition: $\sim Al_{94.7}La_{2.5}Ni_{2.82}$) composition α-Al plus eutectic phase solidifies from the liquid melt, whereas from the hypereutectic liquid melt either primary $Al_{11}La_3$ phase plus eutectic phase or primary $Al_{11}La_3$ and Al_3Ni phases plus eutectic phases precipitates depending upon Ni and La content in the melt. For example, in an $Al_{93.4}Ni_{3.2}La_{3.2}$ alloy the former one and in an $Al_{91.5}Ni_{4.5}La_{4.0}$ alloy the later one precipitates from the alloy melt solidified by the Bridgman technique at a temperature gradient of around 12 K min^{-1} and growth velocity in the range of 0.01–5 mm s^{-1} [21]. The crystallization products of second and third crystallization stages in the present investigation are different from literature [13, 14, 17] may be due to composition difference and difference in processing conditions. In these literatures the report regarding the Ni content is higher (>8 at.%) and Mm content is lower (<5 at.%) than the composition mentioned in this paper. Here, it should be mentioned that the demarcation between the $Al_{11}La_3$ and $Al_{11}Ce_3$ phases is difficult due to their same crystal structure with same space group of *Immm* and similar lattice parameter [22].

Figure 5 shows the isothermal DSC traces of the amorphous $Al_{87.5}Ni_7Mm_5Fe_{0.5}$ at temperatures below the peak of the primary crystallization stage. Generally, an isothermal trace consists of an instrument transient at early times followed by a change that comes from the sample. In order to account for the instrument transient, we record the difference of two traces obtained in similar subsequent measurements on the same sample. The exothermic reaction (Fig. 5) starts after a short incubation time followed by steep rise to an exothermic peak and then a slow decrease in reaction rate leading to tail at higher temperature side. Such asymmetric curve indicates that crystallization takes place for a short nucleation stage due to steep rise of exothermic peak and a prolonged growth stage due to slow reaction rate in the isothermal curve [23]. The Avrami exponent, n, calculated from Johnson–Mehl–Avrami (JMA) [24, 25] transformation kinetics equation, of crystallization of fcc-Al is shown in Fig. 5b. For the range of data between $x = 0.1$ and $x = 0.8$ the average value of n is 1.48 and 1.36 at 145 and 150 °C, respectively. According to Christian's [26] classification this indicates that fcc-Al in

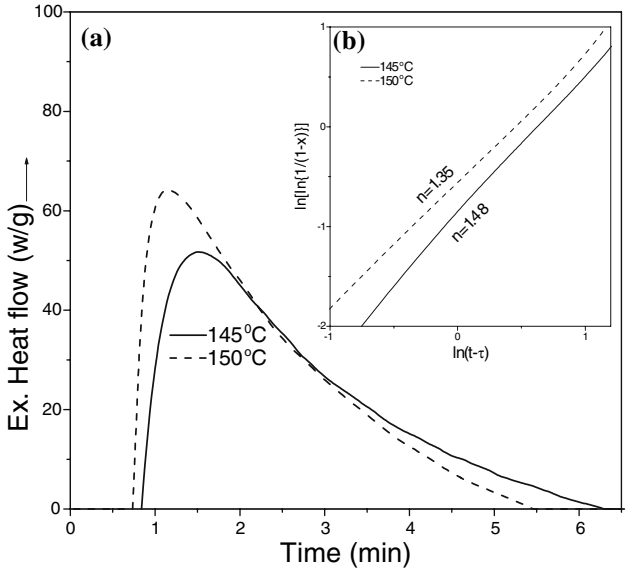

Fig. 5 (**a**) Isothermal DSC curves of amorphous $Al_{87.5}Ni_7Mm_5Fe_{0.5}$ annealed at temperature 145 and 150 °C, and (**b**) in set JMA plots at these temperatures

$Al_{87.5}Ni_7Mm_5Fe_{0.5}$ amorphous matrix grow from small clusters which are already present in the as-melt-spun materials. Also the crystallization takes place by a nucleation stage of shorter duration followed by a prominent growth stage. The growth rate of Al particle may be very sluggish owing to the low diffusivity of the constituent elements in the amorphous phases.

Figure 6 shows the variation of hardness with annealing temperature. Individual ribbons were annealed for 10 min at temperatures starting from room temperature (25 °C) to 480 °C. The heating rate up to the annealing temperature was 100 K/min. The hardness values shown in Fig. 6 are the average of about 10 measurements on each sample and the corresponding error bar is shown for each data point. The hardness values of the ribbon remain nearly same up to 100 °C, after which it increases rapidly up to 260 °C then the hardness remains same or slowly increases up to 320 °C followed by sharp drop of hardness where the second crystallization sets in. The nearly same hardness value up to 100 °C indicates no crystallization or growth of Al-crystals. The increase of hardness with rising temperature is an effect of crystallization and growth of fcc-Al leading to precipitation strengthening of the materials. The crystallization and growth of Al particles enriches the remaining amorphous matrix in solute elements, which is also partially responsible for high hardness with increasing temperature. At the point where the highest hardness is observed the matrix is still amorphous (Fig. 7) while being supersaturated with solute elements. Figure 7 shows the continuous heating DSC curves obtained from the samples annealed for 10 min at 310 °C (solid line) and 340 °C (dotted line). These two temperatures are selected from the points before and after sharp drop of hardness. For the samples annealed at 310 °C, two exothermal stages were observed during subsequent continuous heating indicating that the matrix is still amorphous after annealing at 310 °C for 10 min. The DSC curve (Fig. 7) of this sample shows that the second and the third peak temperatures are 360 and

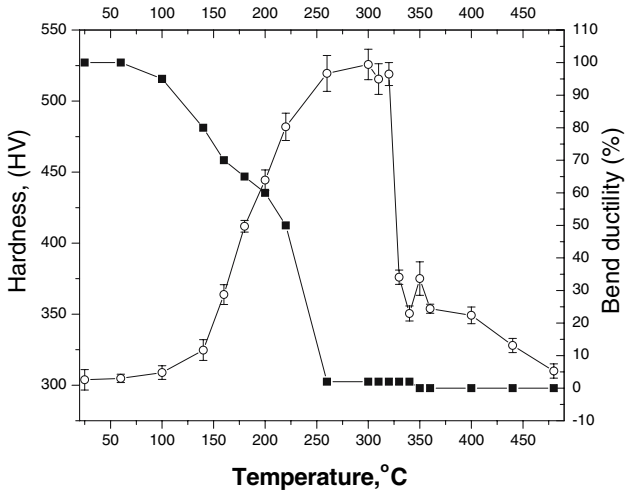

Fig. 6 Variation of microhardness and bend ductility of amorphous $Al_{87.5}Ni_7Mm_5Fe_{0.5}$ melt-spun ribbons at different annealing temperatures. Opened symbols for hardness and closed symbols for bend ductility. Each sample was annealed for 10 min at the indicated temperature

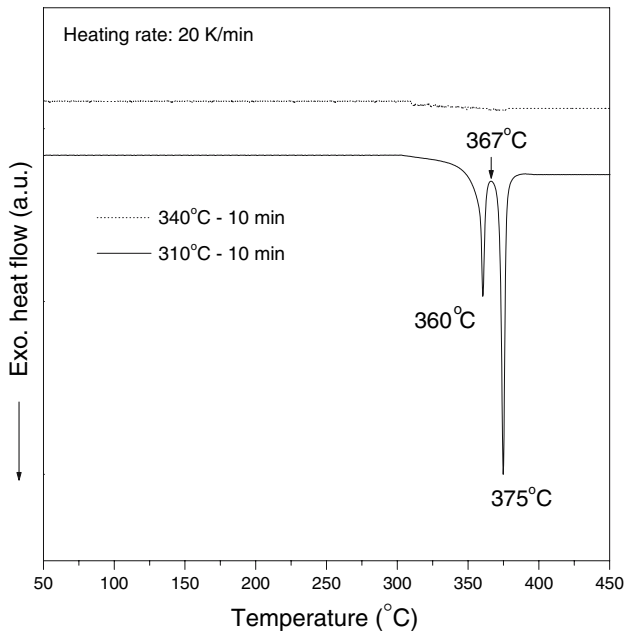

Fig. 7 Continuous heating DSC curve of the $Al_{87.5}Ni_7Mm_5Fe_{0.5}$ alloy after isothermal annealing for 10 min 310 °C (solid line) and 340 °C (dotted line)

375 °C, respectively, that are more than the corresponding peak temperatures when the as-melt-spun ribbon is heated continuously (second and third peak temperatures are 349 and 363 °C, respectively). The higher peak temperatures for the annealed samples show that after primary crystallization the remaining amorphous matrix is enriched in solute elements. For the sample annealed at 340 °C no heat release was observed during subsequent isochronal heating indicating that prior to continuous heating i.e. during annealing the amorphous matrix crystallized completely. Thus, the sharp drop of hardness accounted for the decomposition of amorphous matrix and that leads to precipitation of intermetallic particles from the matrix. With the advancement of crystallization, the hardness slightly increases again due to an increased volume fraction of intermetallic particles. The hardness drops with further increases of temperature may be due to the coarsening of the intermetallic particles. There exists some literatures [11, 27, 28] that report the hardness behaviour in the primary crystallization range but with time in Al–Ni–Ce/La alloys.

Tensile testing is found to be highly sensitive to the surface quality of the ribbons and often gives very variable strength and ductility results. The maximum tensile fracture strength of the as-melt-spun ribbons was found to be in the range of 800–850 MPa with elongation around 15% (Fig. 8). The ribbons show increase of strength with loss of ductility during progress of crystallization. The tensile strength of ribbons annealed at 160 °C for 10 min are in the range of 950–1000 MPa with lower ductility (<10%). At higher annealing temperature the tensile testing could not be carried out due to brittle nature of the ribbons. The tensile testing shows ductility results essentially similar to those obtained by bend testing. Though the bend testing is simple but it is an approximate method of evaluating ductility [27]. These tests are very sensitive to flaws such as surface cracks, inclusions etc. Thus, bend testing is not treated as to determine the absolute ductility values. It is presented (Fig. 6) just to compare the values of as-melt-spun ribbons with annealed one. The ductility is gradually degraded by the presence of increased volume fraction of nano-crystals (α-Al) and is later completely lost when greater hardening occurs due to significant crystallization.

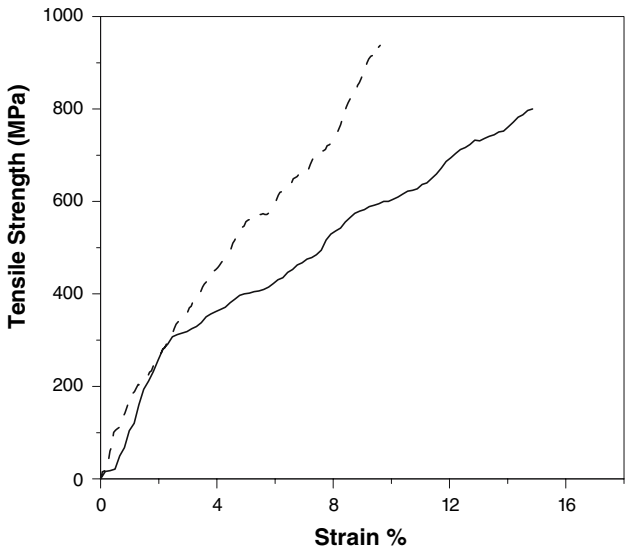

Fig. 8 Tensile stress—elongation curve of $Al_{87.5}Ni_7Mm_5Fe_{0.5}$ alloy; as-melt-spun ribbon (solid line), annealed at 160 °C for 10 min (dotted line)

Conclusions

The as-melt-spun amorphous $Al_{87.5}Ni_7Mm_5Fe_{0.5}$ alloy ribbon observed to be amorphous with good bending ductility. The crystallization behaviour of the as-melt-spun is governed by three exothermic reactions. When the amorphous alloy is heated isochronally the sequence of transformation, as observed by DSC and XRD, is as follows; amorphous (as-melt-spun ribbon) → amorphous + fcc-Al (first crystallization stage) → fcc-Al + $Al_{11}Mm_3$ (second crystallization stage) → fcc-Al + $Al_{11}Mm_3$ + Al_3Ni (third crystallization stage). The crystallization of fcc-Al takes place by short nucleation followed by a prominent growth stage. The observations in regard to second and third stages of crystallization are in contradiction to the earlier report in the literature. The hardness of the amorphous matrix was drastically improved by partially crystallizing the alloy. The sharp increase of hardness from 150 to 260 °C is due to nanoscale precipitation of fcc-Al. The sharp drop in hardness after 320 °C is due to decomposition of the amorphous matrix and formation of intermetallic compounds. With the progress of crystallization, the hardness increases again due to an increased volume fraction of intermetallic particles.

Acknowledgement The authors thank Dr. N. Wanderka, Scientist, Hahn–Meitner–Institute Berlin for her help in performing HRTEM measurements and Director, National Metallurgical Laboratory for his permission to publish the paper.

References

1. Inoue A, Horio Y, Kim YH, Masumota T (1992) Mater Trans JIM 33:669
2. Chen H, He Y, Shiflet GJ (1991) Scripta Metall 25:1421
3. Inoue A (1998) Prog Mater Sci 43:365
4. Kim YH, Inoue A, Masumota T (1991) Mater Trans JIM 32:331
5. Sahoo KL, Wollgarten M, Kim KB, Banhart J (2005) J Mater Res 44:1075
6. Inoue A, Ohtera K, Tsai AP (1988) Jpn J Appl Phys 27:L479
7. Sahoo KL, Wollgarten M, Haug J, Banhart J (2005) Acta Mater 53:3861

8. Kim YH, Hiraga K, Inoue A, Masumota T, Jo HH (1994) Mater Trans JIM 35:293
9. Kim YH, Inoue A, Masumota T (1990) Mater Trans JIM 32:747
10. Ping DH, Hono K, Inoue A (2000) Metall Mater Trans 31A:607
11. Zhong ZC, Jiang XY, Greer AL (1997) Mater Sci Eng A 226–228:531
12. Kim HS, Warren PJ, Cantor B, Lee HR (1999) Nano Struc Mater 11:241
13. Kim TS, Hong SJ, Lee BT (2003) Mater Sci Eng A 363:81
14. Hong SJ, Kim HS, Suryanarayana C, Chun BS (2003) Mater Sci Tech.19:966
15. Inoue A (1998) Prog Mater Sci 43:365
16. Wang SH, Bian XF, Wang HR (2003) Mater Lett 58:539
17. Chang TH, Botten RR (1997) Mater Sci Eng A 226–228:183
18. He Y, Poon SJ, Shiflet GJ (1988) Science 241:1640
19. Allen DR, Foley JC, Perepezko JH (1998) Acta Met 46:431
20. Chen LC, Spaepen F (1991) J Appl Phys 69:679
21. Hawksworth A, Rainforth WM, Jones H (1999) Mater Sci Eng A 262:159
22. Joint committee on powder diffraction standards, files No. 24–501 and 48–1841
23. Chen LC, Spaepen F (1988) Nature 336:336
24. Johnson WA, Mahl RF (1939) Trans Am Inst Min Metal Eng 135:416
25. Avrami M (1941) J Chem Phys 9:177
26. Christian J (1975) The theory of transformation in metals and alloys, Part 1, Equilibrium and general kinetic theory. Pergamon press, Oxford
27. Munoz-Morris MA, Surinach S, Varga LK, Baro MD, Morris DG (2002) Scripta Mater 47:31
28. Kim TS, Hong SJ, Lee BT (2003) Mater Sci Eng A 363:81